Hidden in its color: A molecular-level analysis of the beer's Maillard reaction network

Stefan A. Pieczonka[a,b], Daniel Hemmler[a,b], Franco Moritz[b], Marianna Lucio[b], Martin Zarnkow[c], Fritz Jacob[c], Michael Rychlik[a], Philippe Schmitt-Kopplin[a,b,*]

[a] Chair of Analytical Food Chemistry, Technical University of Munich, Maximus-von-Imhof Forum 2, 85354 Freising, Germany

[b] Research Unit Analytical BioGeoChemistry, Helmholtz Zentrum München, Ingolstaedter Landstraße 1, 85764 Neuherberg, Germany

[c] Research Center Weihenstephan for Brewing and Food Quality, Technical University of Munich, Alte Akademie 3, 85354 Freising, Germany

*corresponding author: schmitt-kopplin@helmholtz-muenchen.de

Abstract

We here report a comprehensive non-targeted analytical approach to describe the Maillard reaction in beer. By Fourier-transform ion cyclotron mass spectrometry (FT-ICR-MS), we were able to assign thousands of unambiguous molecular formulae to the mass signals and thus directly proceed to the compositional space of 250 analyzed beer samples. Statistical data analyses of the annotated compositions showed that the Maillard reaction is one of the driving forces of beer's molecular diversity leading to key compositional changes in the beer metabolome. Different visualization methods allowed us to map the systematic nature of Maillard reaction derived compounds. The typical molecular pattern, validated by an experimental Maillard reaction model system, pervades over 2,800 (40%) of the resolved small molecules. The major compositional changes were investigated by mass difference network analysis. We were able to reveal general reaction sequences that could be assigned to successive Maillard intermediate phase reactions by shortest path analysis.

Keywords: FT-ICR-MS, Maillard reaction, Foodomics, Beer metabolomics, Molecular networking, Mass difference network

1. Introduction

Beer belongs to the oldest fermented beverage in the world (Michel & McGovern, 1993). Thousands of years ago, humankind already commenced to purposefully produce durable and nutrient-rich beverages timely concordant with the domestication of cereals (Dietrich et al., 2020). While the shelf life of beer is notably due to hops constituents, the alcohol content and the stable pH value, the raw material's durability is maintained by reducing the water content. The underlying process of malting was widespread in ancient Egypt, where the good taste of heat-treated cereals already was valued (Meußdoerffer & Zarnkow, 2014). It still represents one of the manifold guided processes that make up modern beer brewing, the complexity of which is mirrored in the diverse molecular composition of beer. Beer can be considered as an exceedingly complex organic mixture in an aqueous solution, to which the brewing process contributes as considerably as the ingredients themselves. The heat treatment of the carbohydrate source is a unique step that notably lifts the molecular complexity of beer from that of other beverages. Malting the grain (steeping, germination, kilning/roasting) leads to a series of chemical reactions that are reflected in the "beer's metabolome".

Brewing science and beer analysis has been integrating empirical knowledge about its chemical composition over centuries (Pieczonka et al., 2021). Using numerous analytical approaches including UHPLC-MS, GC-MS and NMR spectroscopy, both targeted and non-targeted strategies described the beer composition with regard to metabolic profiles characteristic for beer types (Duarte et al., 2004), brewing sites (Almeida et al., 2006), beer quality (Lachenmeier et al., 2005), ageing (Rodrigues et al., 2011) or the evolution of hops derived compounds (Haseleu et al., 2010). Recently, our group was able to demonstrate the power the ultrahigh resolution mass spectrometric approach of flow injection Fourier transform ion cyclotron mass spectrometry (FI-FT-ICR-MS) providing a comprehensive picture of the beer's metabolome (Pieczonka et al., 2020). Out of the resolved molecular diversity, molecular networks of plant secondary metabolites that differentiate beer types and raw materials used could be made visible and characterized. Research on the driving force of chemical changes during the roasting process, the Maillard reaction (MR), is more so dominated by targeted approaches. Brewing research focused on understanding the series of complex reactions by studying reaction mechanisms of certain marker molecules and aroma compounds. For example, 5-hydroxymethyl-2-furfuralaldehyde (HMF) is generated by multiple pathways including caramelization

and the MR starting from numerous possible precursors (Capuano & Fogliano, 2011). By comparison, the formation of maltol, characteristic for eponymous dark malt and beer, only occurs in disaccharide systems favored by stereochemistry and hindered dehydration of respective monosaccharide precursors (Yaylayan & Mandeville, 1994). Many studies followed this approach and studied new non-volatile or aroma active compounds including their formation pathways (Hellwig & Henle, 2010; Hellwig et al., 2016; Mavric & Henle, 2006). However, a comprehensive and holistic approach remains inadequately pursued. Comprehensive and molecular-level detection of Maillard derived compounds in beer forms the basis to describe general reaction sequences, driving forces and key intermediates. It carries the potential to guide the MR related brewing processes towards desired attributes of the beer as Maillard reaction products (MRPs) play a major role in its organoleptic, physical and chemical properties. Melanoidins as MR end products determine the color of beer (Kuntcheva & Obretenov, 1996), they contribute to the stabilization of aroma compounds (Obretenov et al., 2002), have foam stabilizing properties (Lusk et al., 1995) and show anti-oxidative properties (Spreng & Hofmann, 2018). The shelf life of beer is further increased due to the inhibition of bacterial growth (Dack et al., 2017). Overall, beer quality could benefit from optimizing the MR not only towards the formation of a few targeted molecules, but addressing and eventually controlling the entire compositional space, including the many still unknowns.

We have recently developed an analytical pipeline based on high-resolution mass spectrometry and data visualization that allows to comprehensively study the early Maillard reaction network on a molecular level in sugar-amino acid model systems (Hemmler et al., 2019; Hemmler et al., 2017). Studying exact mass differences as proxy for the reactome was shown to be a valuable tool to monitor the formation of MRPs and to better understand their chemical interplay. In this study, we apply this analytical strategy to better understand non-enzymatic browning reactions in beer. We aim to capture the huge diversity of the beer metabolome, assess the contribution of MR products and extract related accurate masses. Visualization and integration of molecular compositions into molecular networks will enable us to capture a comprehensive picture of the Maillard reaction as it may occur in the (bio)chemically complex beer system.

2. Materials and methods

2.1 Beer samples and Maillard model system

A total of 250 samples of bottled beers from over 40 different countries were analyzed. They represent the variety of different beer styles, fermentation types (lager, wheat, craft, geuze, abbey) and raw materials available. The samples were purchased at local grocery stores between 2018 and 2020 and stored at -20 °C prior preparation for analyses.

For the model system, the concentration of 19 amino acids, accessible for derivatization with o-phthaldialdehyde, and 5 saccharides were analyzed in a biological triplicate and technical duplicate of green malt as described in Supplementary Table S1. The concentration of the amino acids and sugars, as described in Supplementary Table S2, were recreated in Milli-Q purified water (Merck Millipore, Darmstadt, Germany) immediately prior to thermal treatment. The concentration of all amino acids added up to 0.12 M and the sum of saccharides' concentration was 0.26 M. The sample was heated in a closed glass vial until the increase in mass features flattened out and the final phase of the MR was reached (20 hours at 100°C). The model system was created and measured in triplicates.

2.2 UV-Vis measurements

The beer samples and Maillard model system were diluted 1:40 in Milli-Q purified water and centrifuged (14.000 rpm, 4 min.). An aliquot of 100 µL of the supernatant was used for UV/Vis analysis in Nunc UV-transparent 96-well microtiter plates (Thermo Fisher Scientific, Waltham, MO, USA). The absorption values at 294 nm and 420 nm were measured on a Multiskan Sky UV-Vis reader (Thermo Fisher Scientific, Waltham, MO, USA) with temperature control (23°C).

2.3 FI-FTICR-MS measurements

High-resolution mass spectra were acquired on a Bruker solariX ion cyclotron resonance Fourier transform mass spectrometer (Bruker Daltonics GmbH, Bremen, Germany) equipped with a 12 Tesla superconducting magnet (Magnex Scientific Inc., Yarton, GB) and a APOLO II ESI source (BrukerDaltonics GmbH, Bremen, Germany) operated in negative ionization mode. To minimize ion suppression while allowing detection of a maximum number of monoisotopic signals, we carefully optimized

sample dilution. Best compromise could be achieved, when beer samples and model systems were diluted 1:500 in methanol prior to injection into the micro electrospray source. The samples were measured over a period of 24 months in randomized order using a representative lager beer as quality control. 80 % of all detected monoisotopic signals could be assigned to a molecular formula within an error range of ± 0.2 ppm and the mass resolution was stable at 400,000 at *m/z* 400 between and within measurement days. The used reagents, sample preparation and instrumental parameters are given in Supplementary Table 3.

2.4 FT-ICR-MS Data processing

The FT-ICR spectra were exported to peak lists with a cut-off signal-to-noise ratio (S/N) of 6 using DataAnalysis 4.2 software. Only singly charged ions were included. Spectra were first externally calibrated by ion clusters of arginine prior to internal calibration by a calibration list of 2000 compositions commonly found in beer. Possible space charge effects were recalibrated by mass difference mapping (Smirnov et al., 2019). Processing and filtration of the peak lists (FT-side loops and isotopologue filtering) were performed by an in-house R-based software tool on basis of single spectra. Peak alignment was performed within a threshold of 0.5 ppm as described by Lucio et al. (2001). Thereby an overall matrix of 11,500 masses was created. To obtain molecular formulae, the accurate masses were subjected to mass difference network (MDiN) analysis using the in-house NetCalc software tool (Tziotis et al., 2011). The network calculation was repeated five times and coinciding formula assignments were kept, which led to approximately 9,500 unambiguous molecular formulae in the CHNOSPCl space. $[M+Cl]^-$ adducts were converted into the respective $[M-H]^-$ ion. Of those, all annotations that are featured in at least three beers were kept for statistical analysis (6,750). A full mass difference statistic was computed on the theoretical neutral masses of each sample. The set of unique mass differences existing within all full mass difference graphs was computed and the relative abundancies of each mass difference was obtained. Mass differences that occurred at least 100 times in a single beer sample (15,500) were used for further statistical analysis (PCA, OPLS) on the relative abundancies of each mass difference within the different samples.

2.5 Statistical analyses

Firstly, we used an unsupervised Principal Component Analysis to separate the beer samples based on the molecular signatures that determine the biggest variance. In the

second step, an OPLS-DA was performed to extract the molecular pattern which correlates with the absorption at 294 nm. The Hotelling's T^2 test (95%) was applied to prohibit the influence of strong outliers on the models. The lists of the most important masses and mass differences were defined choosing the highest loadings values. The top characteristic masses were selected within the 90^{th} percentile (674 masses for each dark and pale beers) and referred to as dark and pale markers in the following, respectively. The goodness of the fit and of the prediction were evaluated with the R2Y and Q^2 values. To exclude overfitting, we computed the p-value of the Cross-Validation Analysis of Variance (CV-ANOVA). The same approach was carried out with the relative abundancies of mass differences occurring in the beer samples. Additionally, based on the robustness of the models, we performed a prevision on the Maillard model system. The recognition of compositional pattern could verify the MR origin of the found patterns and set both models in relation. Those elaborations were done in SIMCA 13.0.3.0 (Umetrics, Umeå, Sweden). The statistical parameters of the beer samples and Maillard model system (Supplementary Table S4) and PCA and OPLS models (Supplementary Table S5) can be found in the Supplementary information.

2.6 Mass difference network analysis

Besides the mass difference network that was used for the annotation of the FT-ICR-MS data (FT-ICR-MS data processing), a second MDiN was created, which includes all compositions found in both the beer samples and the model system. These nodes were connected by edges representing transformations from the Hodge's scheme (Hodge, 1953) and expanded by reactions including MR fission products (Supplementary Table S6). They are referred to as small Maillard intermediate phase reactions and mass differences in the following. In total ~65,000 connections were received. Based on this second network, the nine most significant compositional changes elucidated by OPLS statistical treatment of the first full MDiN were broken down into smaller individual reaction sequences. More precisely, we computed the shortest paths connecting any source-target pair of the statistically significant, composite mass differences using the unweighted Dijkstra algorithm in the Python 3.7 programming environment on a compatible network library (Hagberg et al., 2008). For each statistically significant mass difference, a dominant combination of small reactions of the modified Hodge's scheme was determined. The chronological orders of the individual reactions were compared, giving us a dominant reaction sequence. By

this approach, we received a chronological reaction sequence that build up the ten statistically most significant compositional changes during the MR.

2.7 Data visualization

The marker formulae were depicted in van Krevelen. By plotting H/C versus O/C atomic ratios it is possible to depict common compositional patterns within observations' markers (Hertkorn et al., 2008). The degree of unsaturation of the compositions was calculated as double-bond equivalents (DBE, sum of rings and double bonds in a molecule) and plotted against the number of carbons. A modified Kendrick mass defect analysis (Kim et al., 2003) was applied to visualize the role of dehydration reaction cascades in both marker subsets. The DBEs, modified KMDs and length of homologous series were calculated as described recently (Hemmler et al., 2018; Hemmler et al., 2017). The assignment of corresponding chemical spaces to markers' compositions, their number of nitrogen and their number of oxygen atoms were plotted according to the respective frequency. The developed mass difference network was visualized by the open accessible Gephi Viz Platform (Bastian et al., 2009) using the Force Atlas algorithm.

3. Results

3.1 Contribution of the MR to the beer's molecular complexity

In our study, we investigated the chemical diversity of a total of 250 bottled beer samples that cover the many facets of beer brewing by FI-FT-ICR-MS. As shown in a previous study (Pieczonka et al., 2020) our non-targeted analytical approach can resolve the entire molecular complexity of beer in a single measurement. Covered compounds include carbohydrates, peptides, lipids, polyphenols, hop bitter acids, sulfates and phosphates as well as mostly yet inadequately characterized Maillard reaction products (MRP). The richness and diversity of the selected beer samples capture the great chemical space of the beer metabolome and provide a well-suitable basis to study the contribution of the MR. We were able to assign 7,000 unambiguous molecular compositions to the accurate monoisotopic masses (Fig. 1A) within the sample set reaching from very dark (Fig. 1B) to very pale (Fig. 1C) beers (EBC color values reaching from 5 to 150, Supplementary Table S1). The *m/z* values reached from 100 to 1000. The molecular formulae were annotated in the CHNOSP chemical space and subjected to further statistical analyses.

We used Principal Component Analysis (PCA) to assess the impact of MRPs on the molecular beer composition (Figure 2A). The unsupervised statistical treatment reveals the greatest molecular differences between the beer samples as well as their underlying brewing principles and techniques. The PCA score plot was colored according to each beer's absorption at 294 nm, measured by UV-Vis spectroscopy and reported characteristic to follow the evolution of MR (Yu et al., 2012). The plot reflects the samples' degree of browning with the tendency to lower left positions. Therefore, non-enzymatic browning can be considered to be of major importance for the chemodiversity in beer. It leads to key compositional changes already visible in unsupervised statistics.

We applied a second statistical analysis, a supervised OPLS-DA, to generate in depth knowledge of compositions driving the differentiation of dark beers (Figure 1B) and pale beers (Figure 1C). Compared to PCA, OPLS-DA allowed the extraction of accurate masses without an influence of orthogonal metabolic information, which does not contribute to the compositional changes affected by the MR. The received R2Y-, Q^2- and ANOVA p-value indicate a highly significant multivariate model (Eriksson et al., 2008; Golbraikh & Tropsha, 2002; Westerhuis et al., 2008) (Supplementary information Table S5). The gradient of absorption values, already visible in the PCA and established as driving Y-variable, is reflected in the first component of the OPLS score plot (Figure 2B). The comparison of both statistical models' loading plots shows that the OPLS is capable to extract the same features that drive the MR related separation of the beer samples in the PCA (Figure 2C). We further analyzed an experimental Maillard reaction model system and integrated the results into the OPLS-DA. According to the amino acid and carbohydrate profiles and concentrations of analyzed green malt (Supplementary Table S2), we designed the MR model system, which we heated to 100°C in order to simulate the processes during malting and brewing. To a certain extent, this model represents Maillard reactions between multiple sugars and amino acids in beer. The experimental model system allowed us to validate the assumption that monitoring the absorption at 294 nm can be used to study the MR in beer. The prediction of the model system's position in the OPLS score plot locates it to the far right validating that our OPLS model is capable to recognize the intrinsic nature of Maillard derived complex systems (Figure 2B). The MR molecular pattern in beers, which is extracted by the statistical treatment and classified with regard to the compounds' significance, matches the chemical space of the MR model system

(Supplementary Fig. S2). We could reproduce 80% of the most significant compositions found in beer (90th percentile of most positive loadings) in the saccharide and amino acid experimental model system (Supplementary Figure S2). The overlap between the masses found in beer and those of the model system decreased with decreasing loading values of the respective masses. In comparison, compositions characteristic for pale beers (90th percentile of most negative loadings) showed an overlap of less than ten percent.

3.2 The compositional nature of the MR in beer

The OPLS loadings plot allowed to extract compositions related to the MR from the rich diversity of beer metabolites and rank them according to their significance. To study the molecular pattern of MRPs, we focused on the top ten percent (90th percentile) of the most significant marker compositions for both the dark and pale beer characteristic. Yet, the typical compositional pattern of the Maillard reaction, reported by Hemmler et al. (2017) and reflected in the MR model system, pervades at least 40% (2.800) of all annotations (Supplementary Figure S1).

Several plots and visualizing tools can be used to depict and describe the compositional nature of complex (bio)chemical systems (Hemmler et al., 2019; Hemmler et al., 2018; Hertkorn et al., 2008; Kim et al., 2003). The annotations of the dark beer markers are almost exclusively limited to the CHO (52 %) and CHNO (48 %) space (Figure 3A-I). The number of molecular formulae that contain nitrogen atoms decreased linearly with the number of nitrogen atoms which implies a compositional space built up by chemical kinetics (Figure 3B-I). The frequency of molecular formulae is gaussian-like distributed against the number of oxygen contained, but lacks compositions with less than four oxygen atoms (Figure 3C-I). Compounds with very low oxygen numbers that can be detected by FT-ICR-MS in negative electrospray mode are most commonly annotated as fatty acids or lipids (Pieczonka et al., 2020; Schmitt-Kopplin et al., 2019). Such compositions can be found in the marker masses of pale beers (Figure 3C-II). Overall, in contrast to the dark beer markers, the plots of beer metabolites that are characteristic for pale beers and do not come from the MR do not share a distinct compositional space, as comparatively described in other fermented beverages missing heat load (Gougeon et al., 2009; Roullier-Gall et al., 2014) (Figure 3A-C-II).

Furthermore, the comparison of marker masses of pale and dark beer markers in the van Krevelen diagram shows substantial differences (Figure 3D). The Maillard reaction leads to a highly organized compositional pattern of compounds which is mainly formed through consecutive dehydration, carbonyl cleavage and redox reactions (Hemmler et al., 2018) Interestingly, the extracted molecular formulae of the dark beer marker masses indicate the same compositional pattern. Compositions corresponding to well-known MRPs like 5-hydroxymethylfurfural (HMF, $C_6H_6O_3$), pronyl-lysine ($C_{15}H_{24}N_2O_6$) or Maltosine ($C_{12}H_{18}N_2O_4$) as well as early intermediates like desoxyosones (e.g. $C_6H_{10}O_5$) and Amadori rearrangement products (deoxyhexosylglycine, $C_8H_{15}NO_7$) can be found in both the model system and the dark beer markers. This systematics is contrasted with the van Krevelen diagram of pale beer compounds (Figure 3D-II). The generally more saturated molecular formulae do not cluster in a discrete area. Merely, the areas in the van Krevelen diagram indicate thermolabile lipids and peptides (Pieczonka et al., 2020) which may function as MR precursors. The degree of unsaturation of MR derived compounds, expressed as double-bond equivalents (DBE), follows a highly systematic structure compared to markers for pale beers (Figure 3E). Only a group of early MR intermediates of higher-chain saccharides (e.g. $C_{24}H_{40}O_{20}$, $C_{24}H_{38}O_{19}$, $C_{24}H_{36}O_{18}$ at C>20 and DBE<8) resist the clear, almost linear trend of higher DBEs for higher masses (Fig. 3E-I). The biggest difference between the highly structured MR compositions, which are based on defined chemical reaction cascades, and other beer metabolites are shown in the modified Kendrick mass defect (KMD) plot (Figure 3F). Both, in the CHO and CHNO chemical space homologous series of water elimination reactions can be observed. The maximum length of water elimination cascades equals seven with an average of 3.9. This is in agreement with values for MR models reported in literature (7 and 3.9) (Hemmler et al., 2017) and values computed for our model system (8 and 4.0). By contrast, the pale beer markers do not exceed a homologous series of more than three consecutive dehydration events.

By these visualization methods, we could confirm the MR origin of hundreds to thousands of compositions in beer attributed significant for darker beers in the statistical data evaluation and describe their intrinsic compositional structure. The modified KMD plot furthermore implies that the reaction cascade of the MR is captured in the marker compositions.

3.3 The Maillard reaction molecular network in beer

To get deeper insights into the Maillard reaction cascade that leads to the deciphered molecular complexity, we applied a mass difference network (MDiN) analysis. Based on the relative abundancies of mass differences that connect the elementary compositions of each sample and represent chemical reactions or reaction sequences, both PCA (Figure 2D) and OPLS (Figure 2E) statistical analyses were used. Similar to the statistics on the compositions above, the PCA plot shows a gradient of darkening colors with the tendency to lower positions of the beers in the score plot (negative PC2 values). Using the absorption values of beers at 294 nm as Y-variable in an OPLS-DA, we were able to extract the most significant mass transformations for dark beer samples. This is in agreement with the mass differences (MDs) driving the separation in the PCA (Figure 2F). Again, the MDs match the dominant ones of the Maillard model system (Figure 2E).

These exact mass differences can be equated with changes in the molecular formulae and therefore compositional changes. They describe the compositional change a source compound undergoes to build a target composition. The ten most significant compositional changes are almost exclusively limited to the CHO chemical space and reach from 68 Da to 154 Da. Based on the shifts in the respective molecular formula, there are no single reaction equivalents that describe these changes. Consequently, they rather represent (reaction) sequences of individual smaller compositional changes and are referred to as composite mass differences in the following.

The van Krevelen diagram of the reaction pairs show that higher weight reactants appear in the area of early MR products (Figure 4A). The associated compounds with lower *m/z* values can be assigned to the area of unsaturated advanced MRPs (Figure 4B). Accordingly, source compounds of the composite reactions have higher masses than the target compounds. The most significant reactions could be defined as degradation processes.

To decipher the individual reactions, a MDiN analysis was applied on all annotated compositions (N = 7000). The nodes in the network shown in Fig. 4C represent compositions annotated in both beer samples and the model system. The compositions are connected by edges representing the mass differences typical for the MR intermediate phase. This includes transformations, such as dehydration, decarboxylation, and carbonyl cleavage reactions (full list of 11 transformations see Supplementary Table 1). Due to the lack of a universally applicable nitrogen-containing mass transition, the tenth MD was omitted. We were able to connect the majority

(>95 %) of source-target pairs of the statistically significant composite mass differences by individual small reactions and define the shortest paths by the unweighted Dijkstra algorithm. For each big compositional change, a certain combination of intermediate phase reactions was dominant (Table 1). The chronological order of the respective individual Maillard intermediate phase reactions was compared (Supplementary Figure S3). The order can be assumed to represent the evolution of the composite MR compositional changes. With up to 175 different chronological orders, for each composite mass difference one reaction sequence was very dominant. An overview of the ten most significant compositional changes and their break down into chronological reaction sequences is given in Figure 5. They share a similar structure: all feature a dehydration cascade, whereas most of them end with a decarboxylation reaction. Fission products of early MR intermediates such as glyoxal, methylglyoxal and diacetyl mark the beginning of the reaction sequence in many cases.

4. Discussion

The progress of the early MR was followed by the absorption at 294 nm. The UV absorbance at 294 nm is commonly used to indicate Maillard reaction products of the intermediate phase (Yu et al., 2012). Absorption values of the beer samples measured at 294 nm (MR intermediates) and 420 nm (advanced MR products) showed a very strong correlation (Pearson correlation coefficient: 0.98). Consequently, our identified marker candidates include MRPs from the entire reaction network (initial, intermediate and final MRPs). The MR-correlating compositions lead to a differentiation of the beers already in the first principal components of the unsupervised statistical analysis. It shows that the reaction of sugars and amines define a large part of the beer metabolites. Besides the OPLS statistical parameters (R^2 > 0.92, Q^2 > 0.79 and ANOVA p-value << 0.05), the decreasing coverage of the marker's chemical space by the MR model system with decreasing loading values confirm the power of our approach. The typical Maillard reaction signature (Hemmler et al., 2017) is dominant and shows up to at least 40% of the whole chemical diversity resolved by FT-ICR-MS.

Different plots and visualization techniques confirm that the markers we found represent a highly systematic and distinct chemical space within the big variety of beer metabolites. Consistent with literature findings, the CHNOS chemical space did not significantly contribute to the universal signature of the MR in beer. This agrees with

low cysteine and cystine concentrations reported in malt, wort and beer (Otter & Taylor, 1976). Confirmatory, an inhibiting effect on the progression of the MR and the formation of final MRPs is described for sulfur containing amino acids (Friedman & Molnar-Perl, 1990). The difference in the chemical signature of compositions specific to dark and pale beers could be attributed to their different origins. MRPs arise from chemical reactions, which follow kinetic and thermodynamic laws, and are not influenced by enzymatic catalysis. As already described in model systems (Hemmler et al., 2018), Maillard derived CHNO compositions can carry multiple nitrogen atoms based on multiple condensation reactions of amino compounds to a sugar backbone. These reactions depend on the reactivity of amino acids involved and the MR intermediate's tendency towards carbonyl cleavage, resulting in new reducing ends of the sugar backbone. The formation of such nitrogen-rich compositions are described to accumulate with the progress of the MR (Hemmler et al., 2017). In the complex beer system, involving numerous and interacting amino compounds, we detected compositions with up to four nitrogen atoms (CHN_1O to CHN_4O). Interestingly, we could observe a linear decrease in the composition frequencies with increasing nitrogen number. This agrees with the formation of nitrogen-rich compositions in the later stage of the MR and might confirm the kinetic nature of the dark beer markers. The number of oxygen atoms, not in the focus of previous studies, was also found to be highly systematic. With oxygen numbers exceeding 20 oxygen atoms and mass values over *m/z* 650, both oligosaccharide precursors and condensation reactions can be regarded as important factors in the formation of MRPs in beer. These high-mass compounds also could be classified in the MR scheme. The evolution of the MR is characterized by dehydration reactions, which are reflected in the van Krevelen diagram where early MRP ($1.5<H/C<2$; $0.75<O/C<1$) evolve to highly unsaturated and aromatic compositions ($H/C<1.5$; $O/C<0.5$). The dehydration reactions inevitably come with introducing a DBE to the respective target formula. Both the increasing number of DBEs with higher mass and dehydration cascades for compositions with Kendrick nominal mass > 400 reinforce the meaning of higher mass, non-volatile MRPs in the complex food system.

Studying exact mass differences, which represent certain compositional changes, we were able to reveal general and conceptual reaction sequences that can describe a part of the Maillard reaction in beer. Condensation reactions lead to compounds with higher mass and lead to a change in the composition, which always depends on both

the carbonyl and amino compounds. Although the condensation of glycine ($C_2H_5NO_2$) and isoleucine ($C_6H_{13}NO_2$) with a carbonyl moiety are very similar in their underlying reaction mechanism, they lead to different compositional changes (C_2H_3NO and $C_6H_{10}NO$, respectively). The same is true for the condensation and interaction of MR intermediates. Other reactions like a simple dehydration or glycation are characteristic to the MR but not specific as a multitude of biochemical transformations includes a loss of water or glycation as well. Accordingly, compositional changes that neither depend on amino acids nor correspond to the condensation of complex intermediates or very simple reactions were to be expected.

Therefore, the ten most significant compositional changes are changes including CHO-transformations coming with a loss of mass. Consequently, at this point, our data do not allow drawing conclusions about the role of single amino compounds but describe the complex system holistically. What was found to be statistically significant can be referred to very general chemical changes that early MRPs or intermediates of diverse origins undergo to build a Maillard reaction end product. By our network and shortest path approach, we furthermore were able to decipher the combination and chronological order of Maillard intermediate phase reactions that match these compositional changes. All intermediates were found in either beer or the Maillard model system and despite of hundreds of possible combinations, the chronological order was consistent within the source and target pairs. This leads us to regard the results of the network approach as reaction sequences.

These sequences share a common inherent structure: Starting with the condensation of a small MR fission product, a dehydration cascade and finally a decarboxylation reaction occurs. These fission products like glyoxal, methylglyoxal or diacetyl arise from retro-aldolization of sugar molecules or cleavage of respective dicarbonyls (Hollnagel & Kroh, 2000). Dehydration cascades are well described to play a major role in the formation of MRPs. In several ribose-amino acid model systems, we were able to highlight the role of early diketosamine formation and its subsequent degradation in the MR (Hemmler et al., 2018). Molecular formulae equivalent to six consecutive dehydration products could be described. Our presented results indicate that such a degradation process might also be caused by the condensation of a fission product, when describing a complex system in general. In the context of the MR, loss of CO_2 likely occurs due to a α-dicarbonyl assisted oxidative decarboxylation (e.g.

Strecker degradation) (Yaylayan, 2003). In this case, the resulting imine is hydrolyzed to give the so-called Strecker aldehyde. The hydrolysis reaction leads to the loss of the specific amino acid residue at the initial dicarbonyl unit. These reactions would be no longer tangible for our general approach. Purely thermally induced decarboxylation reactions, on the other hand, could occur during the roasting process. They require very high temperatures (> 200°C) (Bagdonaite et al., 2008) and thus naturally happen at the end of the heating process and reaction sequences. It is worth noting that the presented pathways and their interpretation are restricted to compositional information obtained by accurate mass measurements. They describe very general and conceptual patterns within a complex food system. Mechanistic studies including various model systems, resolved in time, should be performed to fully understand the reaction sequences we proposed to describe the MR in beer.

In industrial practice, the extensive chemical changes that are associated with the heat load are usually monitored by the unspecific reaction of 2-thiobarbituric acid (TBA) (Guillén-Sans & Guzmán-Chozas, 1998). It is based on the photometric tracking of the reaction of TBA with dicarbonyl functions. However, the origin of the dicarbonyls (e.g. MR or lipid oxidation) and their follow-up reactions cannot be differentiated. By comparison, we recorded over 2,500 compositions that describe the MR in beer comprehensively alongside the reaction network leading to such a multitude of MRPs. Our analytical approach may offer a unique method to guide MR related brewing processes, such as malting and boiling, towards desired attributes of the final beer end product. Having the opportunity to resolve the Maillard reaction cascades and resulting molecular complexity, effects of changed kilning or roasting parameters can be monitored as well as the progress of the MR throughout the whole brewing process.

5. Conclusion

Overall, this study reports a comprehensive analytical approach addressing the great variety of MR-derived products in a complex food system, the description of their compositional nature and the general reaction cascades that lead to the diversity observed. It contributes to the better understanding of the complex molecular processes involved in the MR and might be a starting point for potential process development and quality control in both malting and brewing industry.

6. Conflict of interest statement

This research did not receive any specific grant from funding agencies in the public, commercial, or not-for-profit sectors. The authors declare that they have no known competing financial interests or personal relationships that could have appeared to influence the work reported in this paper.

Figures

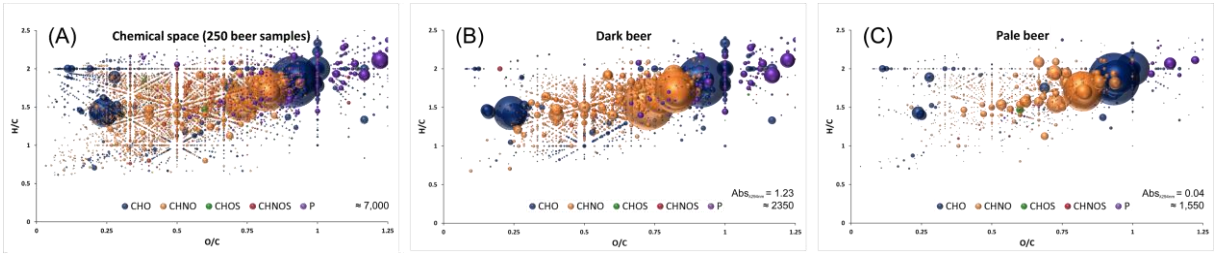

Figure 1. Van Krevelen diagram of molecular formula annotations found in 250 beer samples (A), the darkest (B) and palest (C) beer sample. Color code: CHO blue; CHNO orange; CHOS green; CHNOS red; P purple. Neutral molecular formulae are plotted. The bubble size indicates the mean relative intensities of corresponding peaks in the spectra.

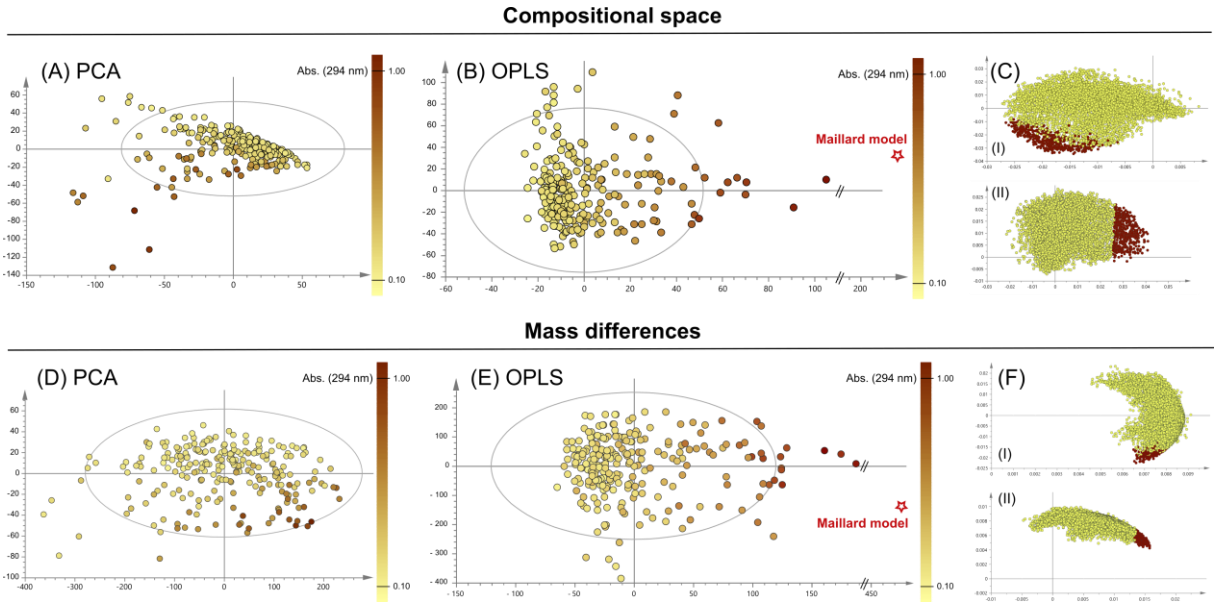

Figure 2. Score plot of the PCA (A) and OPLS (B) analysis of the compositional space of 250 beer samples and the corresponding loading plots (C-I, PCA) (C-II, OPLS). Score plot of the PCA (D) and OPLS (E) analysis of the computed mass differences in 250 beer samples and the corresponding loading plots (F-I, PCA) (F-II, OPLS). The position of the beer samples is marked by dots colored according to their absorption at 294 nm. The prediction of the Maillard model system in the OPLS models (B and E) is highlighted as a red star. Masses in the PCA-loading plot (C-I and F-I) that match the most significant masses for dark beers in the OPLS-loading plot (C-II and F-II) are colored brown.

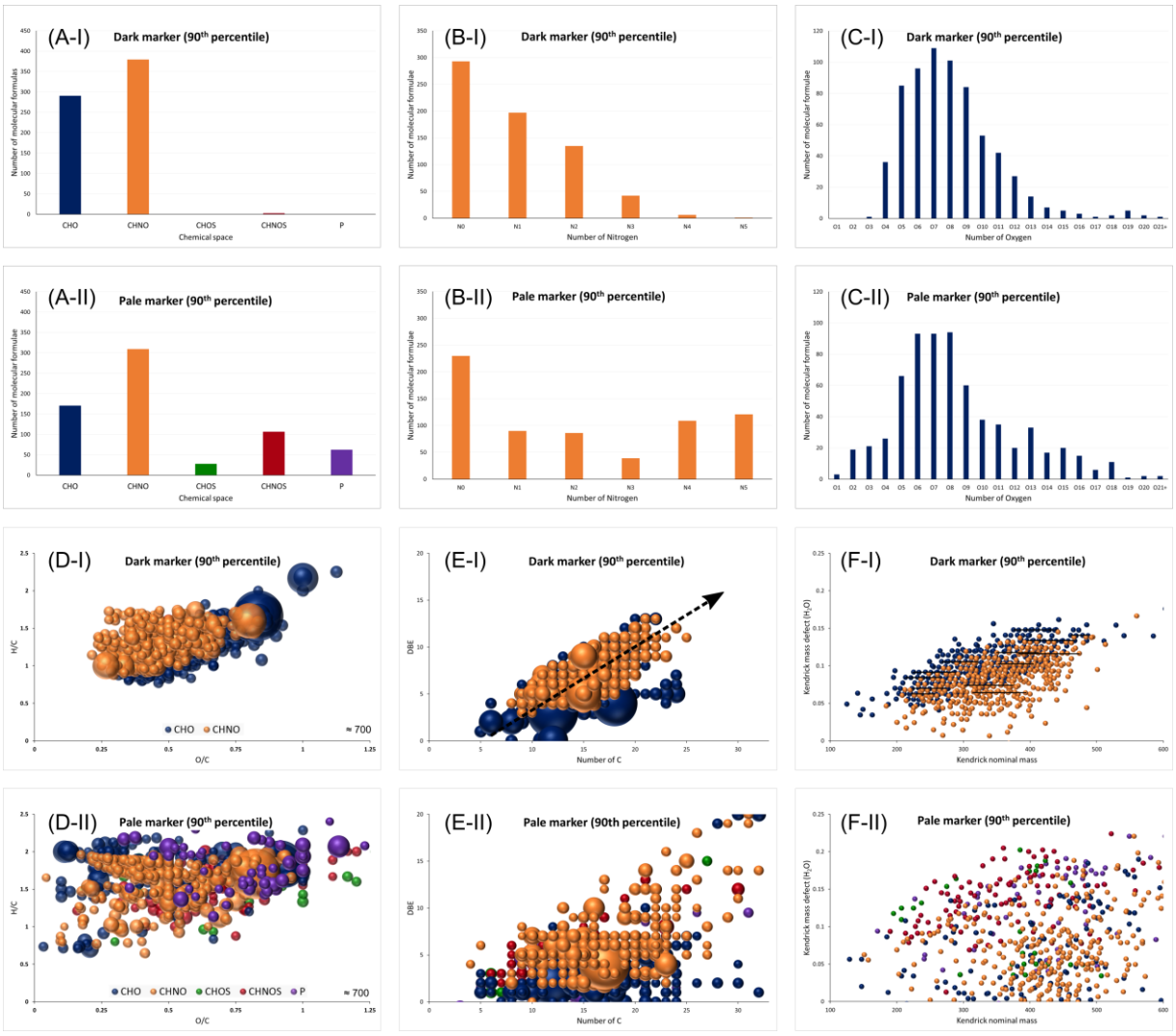

Figure 3. Comparison of dark (I) and pale (II) beer marker molecular formulae by different visualizing plots (A-F). Number of annotations in the chemical spaces (A), number of nitrogen atoms (B), number of oxygen atoms (C), Van Krevelen diagram (D), Double bond equivalents against Number of Carbon atoms (E) and Kendrick mass defect plot with H_2O homologous series (F). Color code: CHO blue; CHNO orange; CHOS green; CHNOS red; P purple. Neutral molecular formulae are plotted. The bubble size indicates the mean relative intensities of corresponding peaks in the spectra (D, E). Rising DBE with higher masses for dark markers is indicated in (E-I). Homologous series of H_2O-reactions are marked exemplary in the KMD plot (F-I). The intrinsic systematic pattern of dark beer markers is opposed to non-systematic annotations of the pale marker masses.

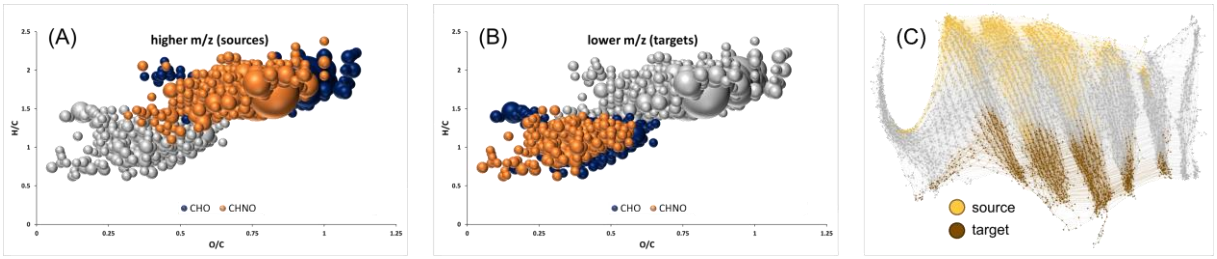

Figure 4. Van Krevelen diagrams of compositions connected by the ten most significant mass differences for dark beers (A and B) and their breakdown into small reaction series by a mass difference network (C). Higher mass values (A) and lower mass values (B) of the mass pairs. The entirety of compositions is in the background in gray. The lower left position of low *m/z* values indicate degradation reaction sequences. Nodes in the mass difference network (C) represent all annotated compositions connected by edges representing small Maillard intermediate phase reactions (Supplementary Table S6). Sources and targets of the statistically most significant big composite mass differences are colored.

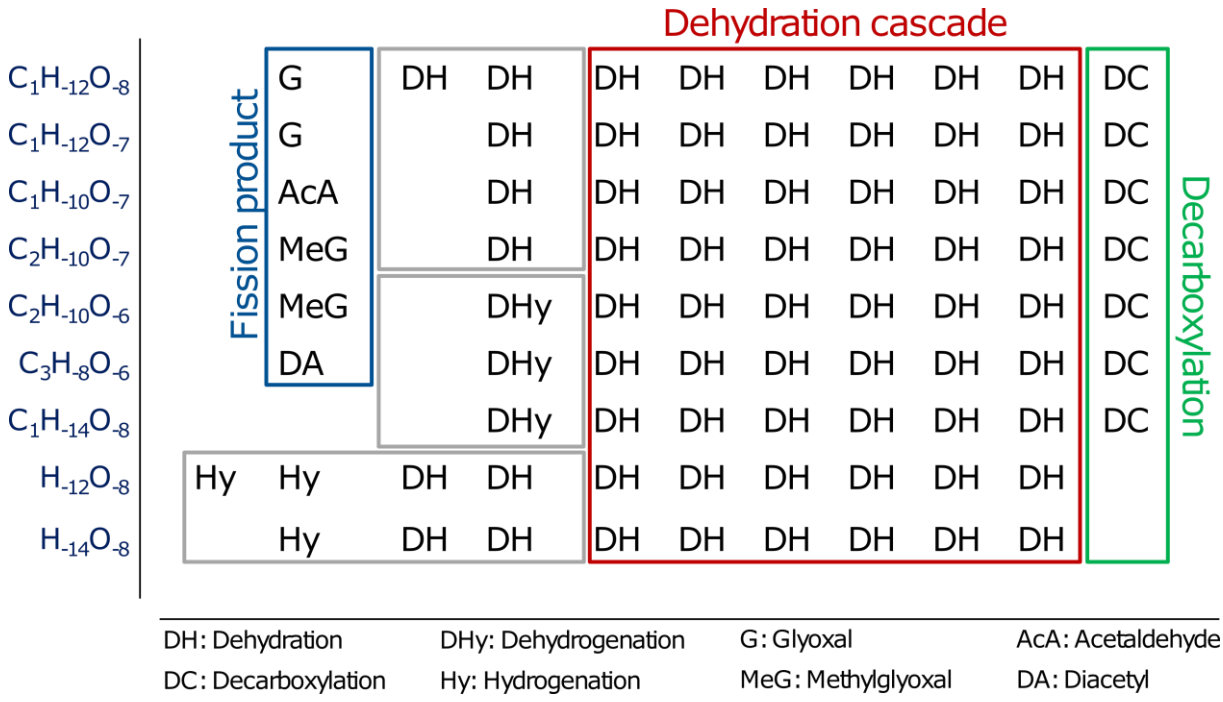

Figure 5. Reaction sequences of the ten most significant compositional changes during the MR in beer. All reaction sequences feature a dehydration cascade. In many cases, MR fission products start the reaction sequence, which ends with a decarboxylation reaction. The compositional change of hydrogenation ($+H_2$) does not indicate the involvement of elemental hydrogen, but a reductone/dehydroreductone reactional environment.

Tables

Table 1. The ten most significant compositional changes during the MR in beer and their break down into small reactions.

loading	Δ *m/z*	formula	frequency	Decomposition into individual MDs	% of shortest paths
0.01581	-128.053	$C_1H_{-12}O_{-8}$	543	Dehydration (8), Glyoxal, Decarboxylation	64
0.01576	-140.053	$H_{-12}O_{-8}$	714	Dehydration (8), Hydrogenation (2)	65
0.01576	-142.069	$H_{-14}O_{-8}$	576	Dehydration (8), Hydrogenation	82
0.01571	-98.0427	$C_2H_{-10}O_{-7}$	685	Dehydration (7), Methylglyoxal	75
0.01566	-110.043	$C_1H_{-10}O_{-7}$	879	Dehydration (7), Acetaldehyde, Decarboxylation	65
0.01565	-112.058	$C_1H_{-12}O_{-7}$	722	Dehydration (7), Glyoxal, Decarboxylation	66
0.01551	-82.0477	$C_2H_{-10}O_{-6}$	890	Dehydration (6), Methylglyoxal, Dehydrogenation, Decarboxylation	83
0.01549	-68.0321	$C_3H_{-8}O_{-6}$	830	Dehydration (6), Diacetyl, Dehydrogenation, Decarboxylation	94
0.01549	-154.069	$C_{-1}H_{-14}O_{-8}$	746	Dehydration (6), Dehydrogenation, Decarboxylation	90
0.01543	-93.0637	$C_1H_{-11}N_1O_{-5}$	861	-	-

553 Almeida, C., Duarte, I. F., Barros, A., Rodrigues, J. E., Spraul, M., & Gil, A. M. (2006). Composition of
554 beer by 1H NMR spectroscopy: effects of brewing site and date of production. *J. Agric. Food*
555 *Chem., 54*, 700-706.

556
557 Bagdonaite, K., Derler, K., & Murkovic, M. (2008). Determination of acrylamide during roasting of
558 coffee. *J. Agric. Food Chem., 56*, 6081-6086.

559
560 Bastian, M., Heymann, S., & Jacomy, M. (2009). *Gephie: an open source software for exploring and*
561 *manipulating networks* International AAAI Conference on Weblogs and Social Media,

562
563 Capuano, E., & Fogliano, V. (2011). Acrylamide and 5-hydroxymethylfurfural (HMF): A review on
564 metabolism, toxicity, occurrence in food and mitigation strategies. *LWT-Food Sci. Technol.,*
565 *44*, 793-810.

566
567 Dack, R. E., Black, G. W., Koutsidis, G., & Usher, S. J. (2017). The effect of Maillard reaction products
568 and yeast strain on the synthesis of key higher alcohols and esters in beer fermentations.
569 *Food Chem., 232*, 595-601.

570
571 Dietrich, L., Götting-Martin, E., Hertzog, J., Schmitt-Kopplin, P., McGovern, P. E., Hall, G. R., Petersen,
572 W. C., Zarnkow, M., Hutzler, M., Jacob, F., Ullman, C., Notroff, J., Ulbrich, M., Flöter, E., Heeb,
573 J., Meister, J., & Dietrich, O. (2020). Investigating the function of Pre-Pottery Neolithic stone
574 troughs from Göbekli Tepe – An integrated approach. *J. Archaeol. Sci. Rep, 34*, 1-20.

575
576 Duarte, I. F., Barros, A., Almeida, C., Spraul, M., & Gil, A. M. (2004). Multivariate Analysis of NMR and
577 FTIR Data as a Potential Tool for the Quality Control of Beer. *J. Agric. Food Chem., 52*, 1031-
578 1038.

579
580 Eriksson, L., Trygg, J., & Wold, S. (2008). CV-ANOVA for significance testing of PLS and OPLS models. *J.*
581 *Chemometrics, 22*, 594-600.

582
583 Friedman, M., & Molnar-Perl, I. (1990). Inhibition of browning by sulfur amino acids. 1. Heated amino
584 acid-glucose systems. *J. Agric. Food Chem., 38*(8), 1642-1167.

585
586 Golbraikh, A., & Tropsha, A. (2002). Beware of q2! *J. Mol. Graph. Model., 20*, 269-276.

587
588 Gougeon, R. D., Lucio, M., Frommberger, M., Peyron, D., Chassagne, D., Alexandre, H., Feuillat, F.,
589 Voilley, A., Cayot, P., Gebefügi, I., Hertkorn, N., & Schmitt-Kopplin, P. (2009). The chemical
590 diversity of wines can reveal a metabologeography expression of cooperage oak wood. *PNAS,*
591 *106*, 9174-9179.

592
593 Guillén-Sans, R., & Guzmán-Chozas, M. (1998). The Thiobarbituric Acid (TBA) Reaction in Foods: A
594 Review. *Crit. Rev. Food Sci. Nutr., 38*(4), 315-330.

595

596 Hagberg, A. A., Schult, D. A., & Swart, P. J. (2008). Exploring network structure, dynamics, and
597 function using networkx. Proceedings of the 7th Python in Science Conference (SciPy2008),
598 Pasadena, CA.

599
600 Haseleu, G., Lagemann, A., Stephan, A., Intelmann, D., Dunkel, A., & Hofmann, T. (2010). Quantitative
601 sensomics profiling of hop-derived bitter compounds throughout a full-scale beer
602 manufacturing process. *J. Agric. Food Chem., 58*(13), 7930-7939.

603
604 Hellwig, M., & Henle, T. (2010). Formyline, a new glycation compounds from the reaction of lysine
605 and 3-deoxypentosone. *Eur. Food Res. Technol., 230*(6), 903-914.

606
607 Hellwig, M., Witte, S., & Henle, T. (2016). Free and protein-bound Maillard reaction products in beer:
608 method development and a survey of different beer types. *J. Agric. Food Chem., 64*, 7234-
609 7243.

610
611 Hemmler, D., Gonsior, M., Powers, L. C., Marshall, J. W., Rychlik, M., Taylor, A. J., & Schmitt-Kopplin,
612 P. (2019). Simulated sunlight selectively modifies Maillard reaction products in a wide array
613 of chemical reactions. *Chem. Eur. J.*

614
615 Hemmler, D., Roullier-Gall, C., Marshall, J. W., Rychlik, M., Taylor, A. J., & Schmitt-Kopplin, P. (2018).
616 Insights into the Chemistry of Non-Enzymatic Browning Reactions in Different Ribose-Amino
617 Acid Model Systems. *Sci. Rep., 8*, 1-9.

618
619 Hemmler, D., Roullier-Gall, C., Marshall, J. W., Rychlik, M., Taylor, A. J. T., & Schmitt-Kopplin, P.
620 (2017). Evolution of complex Maillard chemical reactions, resolved in time. *Sci. Rep., 7*(1),
621 3227-3233.

622
623 Hertkorn, N., Frommberger, M., Witt, M., Koch, B. P., Schmitt-Kopplin, P., & Perdue, E. M. (2008).
624 Natural organic matter and the event horizon of mass spectrometry. *Anal. Chem., 80*, 8908-
625 8919.

626
627 Hodge, J. E. (1953). Dehydrates Foods, Chemistry of Browning Reactions in Model Systems. *J. Agric.*
628 *Food Chem., 1*, 928-943.

629
630 Hollnagel, A., & Kroh, L. W. (2000). Degradation of oligosaccharides in nonenzymatic browning by
631 formation of a- dicarbonyl compounds via a "peeling off" mechanism. *J. Agric. Food Chem.,*
632 *48*, 6219-6226.

633
634 Kim, S., Kramer, R. W., & Hatcher, P. G. (2003). Graphical Method for Analysis of Ultrahigh-Resolution
635 Broadband Mass Spectra of Natural Organic Matter, the Van Krevelen Diagram. *Anal. Chem.,*
636 *75*, 5336-5344.

637
638 Kuntcheva, M. T., & Obretenov, T. D. (1996). Isolation and characterization of melanoidins from beer.
639 *Z. Lebensm. Unters. Forsch., 202*(3), 238-243.

640

Lachenmeier, D. W., Frank, W., Humpfer, E., Schäfer, H., Keller, S., Mortter, M., & Spraul, M. (2005). Quality control of beer using high-resolution nuclear magnetic resonance spectroscopy and multivariate analysis. *Eur. Food Res. Technol., 220*, 215-221.

Lucio, M., Fekete, A., Frommberger, M., & Schmitt-Kopplin, P. (2001). Metabolomics: High-Resolution Tools Offer to Follow Bacterial Growth on a Molecular Level. In F. J. de Bruijn (Ed.), *Handbook of Molecular Microbial Ecology I: Metagenomics and Complementary Approaches* (pp. 683-695). John Wiley & Sons.

Lusk, L. T., Goldstein, H., & Ryder, D. (1995). Independent role of beer proteins, melanoidins and polysaccharides in foam formation. *J. Am. Soc. Brew. Chem., 53*(3), 93-103.

Mavric, E., & Henle, T. (2006). Isolation and identification of 3,4-dideoxypentosulose as specific degradation product of oligosaccharides with 1,4-glycosidic linkages. *Eur. Food Res. Technol., 223*, 803-810.

Meußdoerffer, F., & Zarnkow, M. (2014). *Das Bier. eine Geschichte von Hopfen und Malz* (Vol. 2nd Ed.). Beck.

Michel, R. H., & McGovern, P. E. (1993). The first wine & beer. Chemical detection of ancient fermented beverages. *Anal. Chem., 65*(8), 408-413.

Obretenov, T. D., Demyttenaere, J., Abbaspour-Tehrani, K., Adams, A., Kersiene, M., & De Kimpe, N. (2002). Flavor realease in the presence of melanoidins prepared from L-(+)-ascorbic acid and amino acids. *J. Agric. Food Chem., 50*, 4244-4250.

Otter, G. E., & Taylor, L. (1976). The determination of amino acids in wort, beer and brewing materials using gas chromatography. *J. Inst. Brew., 82*, 264-269.

Pieczonka, S. A., Lucio, M., Rychlik, M., & Schmitt-Kopplin, P. (2020). Decomposing the molecular complexity of brewing. *NPJ Sci. Food, 4*(11), 1-10.

Pieczonka, S. A., Rychlik, M., & Schmitt-Kopplin, P. (2021). Metabolomics in Brewing Research. In A. Cifuentes (Ed.), *Comprehensive Foodomics* (Vol. 2, pp. 116-128). Elsevier.

Rodrigues, J. A., Barros, A. S., Carvalho, B., Brandão, T., & Gil, A. M. (2011). Probing beer aging chemistry by nuclear magnetic resonance and multivariate analysis. *Analytica Chimica Acta, 702*, 178-187.

Roullier-Gall, C., Witting, M., Gougeon, R. D., & Schmitt-Kopplin, P. (2014). High precision mass measurements for wine metabolomics. *Front. Chem., 2*(102), 1-9.

Schmitt-Kopplin, P., Hemmler, D., Moritz, F., Gougeon, R. D., Lucio, M., Meringer, M., Müller, C., Harir, M., & Hertkorn, N. (2019). Systems chemical analytics: introduction to the challenges of chemical complexity analysis. *Faraday Discuss., 218*, 9-28.

686
687 Smirnov, K. S., Forcisi, S., Moritz, F., Lucio, M., & Schmitt-Kopplin, P. (2019). Mass difference maps
688 and their application for the recalibration of mass spectrometric data in nontargeted
689 metabolomics. *Anal. Chem., 91*, 3350-3358.
690
691 Spreng, S., & Hofmann, T. (2018). Activity-guided identification of *in vitro* Antioxidants in beer. *J.*
692 *Agric. Food Chem., 66*, 720-731.
693
694 Tziotis, D., Hertkorn, N., & Schmitt-Kopplin, P. (2011). Kendrick-analogous network visualization of
695 ion cyclotron resonance fourier transform mass spectra: improved options for the
696 assignment of elemental compositions and the classification of organic molecular complexity.
697 *Eur. J. Mass Spectrom., 17*, 415-421.
698
699 Westerhuis, J. A., Hoefsloot, H. C. J., Smit, S., Vis, D. J., Smilde, A. K., van Velzen, E. J. J., van
700 Duijnhoven, J. P. M., & van Dorsten, F. A. (2008). Assessment of PLSDA cross validation.
701 *Metabolomics, 4*, 81-89.
702
703 Yaylayan, V. A. (2003). Recent adcances in the chemistry of Strecker degradation and Amadori
704 rearrangement: implications to aroma and color formation. *Food Sci. Technol., 9*(1), 1-6.
705
706 Yaylayan, V. A., & Mandeville, S. (1994). Stereochemical control of maltol formation in Maillard
707 reaction. *J. Agric. Food Chem., 42*, 771-775.
708
709 Yu, X., Zhao, M., Hu, J., Zeng, S., & Bai, X. (2012). Correspondence analysis of antioxidant activity and
710 UV-Vis absorbance of Maillard reaction products as related to reactants. *Food Sci. Technol.,*
711 *46*, 1-9.
712
713